Part I
Fundamentals: Active Species, Mechanisms, Reaction Pathways

Photocatalysis and Water Purification: From Fundamentals to Recent Applications, First Edition. P. Pichat.

1
Identification and Roles of the Active Species Generated on Various Photocatalysts

Yoshio Nosaka and Atsuko Y. Nosaka

TiO_2 photocatalysts have been utilized for the oxidation of organic pollutants [1–5]. For further practical applications, the improvement in the photocatalytic efficiency and the extension of the effective wavelength of the irradiation light are desired. From this point of view, better understanding of the primary steps in photocatalytic reactions is prerequisite to develop prominent photocatalysts. The properties of TiO_2 and the reaction mechanisms in molecular level have been reviewed recently [6]. Therefore, this chapter describes briefly active species involved in the photocatalytic reactions for bare TiO_2 and TiO_2 modified for visible-light response, that is, trapped electrons, superoxide radical ($O_2^{\bullet -}$), hydroxyl radical ($OH^{\bullet}$), hydrogen peroxide (H_2O_2), and singlet oxygen ($^1O_2$).

1.1
Key Species in Photocatalytic Reactions

Since the photocatalytic reactions proceed usually with oxygen molecules (O_2) in air, the reduction of oxygen would be the important process in photocatalytic reduction. On the other hand, taking into account that the surface of TiO_2 photocatalysts is covered with adsorbed water molecules in usual environments and that photocatalysts are often used to decompose pollutants in water, oxidation of water would be the important process in photocatalytic oxidation. As shown in Figure 1.1, when O_2 is reduced by one electron (Eq. (1.1)), it becomes a superoxide radical ($O_2^{\bullet -}$) that is further reduced by one electron (Eq. (1.2)) or reacts with a hydroperoxyl radical ($HO_2^{\bullet}$, i.e., protonated $O_2^{\bullet -}$) to form hydrogen peroxide (H_2O_2). The latter reaction is largely pH dependent because the amount of $HO_2^{\bullet}$, whose p*K*a is 4.8, changes largely at pH around neutral [7]. One-electron reduction of H_2O_2 (Eq. (1.3)) produces hydroxyl radical ($OH^{\bullet}$). In the field of radiation chemistry, it is well documented that $OH^{\bullet}$ is produced by one-electron oxidation of H_2O with ionization radiation. However, the formation of $OH^{\bullet}$ in the photocatalytic oxidation process has not been confirmed,

Photocatalysis and Water Purification: From Fundamentals to Recent Applications, First Edition. P. Pichat.

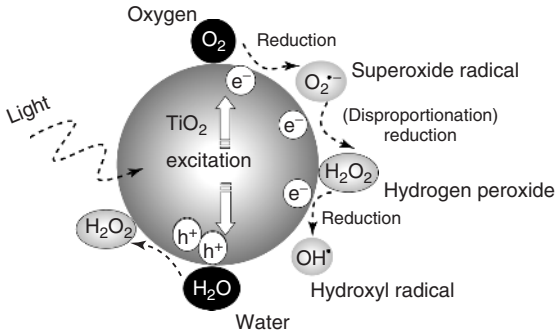

Figure 1.1 One-electron reduction steps of oxygen to OH radical and two-electron oxidation step of water to H_2O_2 observed in the TiO_2 photocatalyst.

as described later.

$$O_2 + e^- \rightarrow O_2^{\bullet-} \tag{1.1}$$

$$O_2^{\bullet-} + 2H^+ + e^- \rightarrow H_2O_2 \tag{1.2}$$

$$H_2O_2 + H^+ + e^- \rightarrow OH^\bullet + H_2O \tag{1.3}$$

Figure 1.2 shows the standard potentials [8] for the one-electron redox of active oxygen species as a function of pH of the solution. The conduction band (CB) bottom for anatase and rutile TiO_2 along with valence band (VB) top of TiO_2 is also depicted. The p*K*a values for H_2O_2 and $OH^\bullet$ are 11.7 and 11.9, respectively [7]. Therefore, the linear lines showing pH dependence in Figure 1.2 change the inclination at the individual pH. It is notable that in the pH range between 10.6 and 12.3, one-electron reduction resulting in $OH^\bullet$ formation (Eq. (1.3)) occurs at a higher potential than that resulting in H_2O_2 formation (Eq. (1.2)). As commonly known, the potential of the VB of TiO_2 is low enough to oxidize H_2O, suggesting the possibility of the formation of $OH^\bullet$. However, the potentials in the figure are depicted based on the free energy change in a homogeneous aqueous solution. Therefore, it does not always mean that the one-electron oxidation of H_2O by VB holes at the surface of TiO_2 solid takes place in the heterogeneous system. Since the oxidation of H_2O to H_2O_2 and O_2 is also possible, only the potential difference between VB and $OH^\bullet$ should not be used easily for explaining the possibility of the formation of $OH^\bullet$. The competition between OH-radical-mediated reaction versus direct electron transfer has been studied as the effect of fluoride ions on the photocatalytic degradation of phenol in an aqueous TiO_2 suspension [9]. Under a helium atmosphere and in the presence of fluoride ions, phenol is significantly degraded, suggesting the occurrence of a photocatalytically induced hydrolysis [9].

Primary intermediates of water photocatalytic oxidation at the TiO_2 in aqueous solution were investigated by *in situ* multiple internal reflection infrared (MIRIR) absorption combined with the observation of photoluminescence from trapped holes [10]. The reaction is initiated by a nucleophilic attack of a H_2O molecule on a photogenerated hole at a surface two hold coordinated O site to form [TiO$^\bullet$HO–Ti].

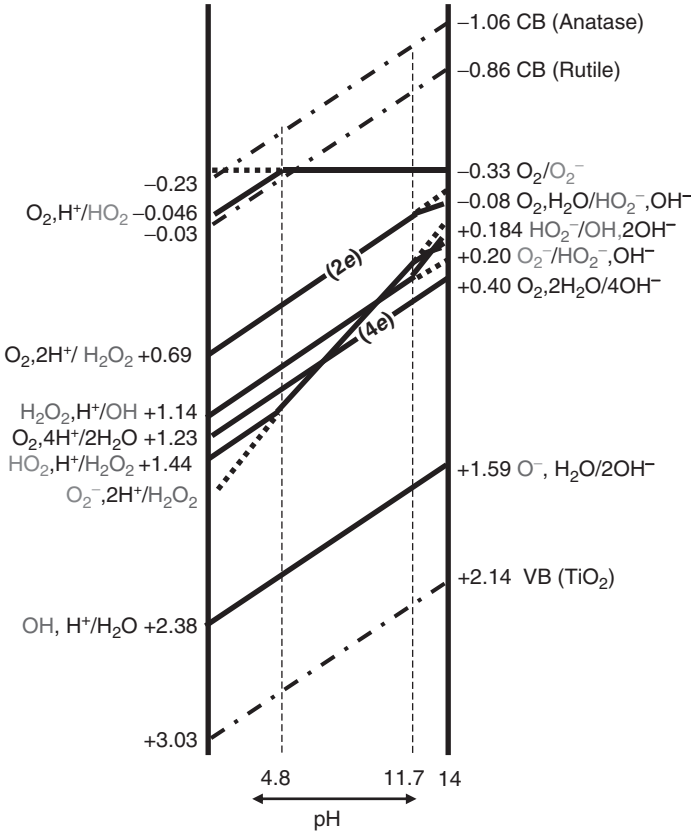

Figure 1.2 The standard potentials for the one-electron redox of active oxygen species along with the energy bands of TiO_2 as a function of pH of the solution. All redox couples are one-electron process except for those indicated with 2*e* and 4*e*.

A plausible reaction scheme is shown in Figure 1.3. Detailed investigations revealed the presence of TiOOH and TiOOTi as primary intermediates of the oxygen photoevolution reaction. This means that water is oxidized to form hydrogen peroxide adsorbed on TiO_2 surface, but the formation of OH radical in the oxidation process of water was denied.

Ultraviolet photoelectron spectroscopy (UPS) studies showed that the top of the O-2p levels for surface hydroxyl groups (Ti–OH) at the rutile TiO_2 (100) face is about 1.8 eV below the top of the VB at the surface [11]. This implies that surface hydroxyl groups cannot be oxidized by photogenerated holes in the VB. On the basis of the electronic structure of surface-bound water obtained from the data reported in the literature of X-ray photoelectron spectroscopy (XPS) study, it is evidenced that water species specifically adsorbed on terminal (surface) Ti atoms cannot be photooxidized under UV illumination [12]. The photogenerated VB free holes are favorably trapped at the terminal oxygen ions of the TiO_2 surface $(O^{2-})_s$

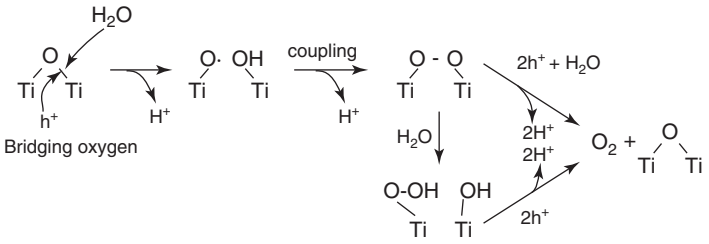

Figure 1.3 Reaction scheme for the oxygen photoevolution reaction on TiO_2 (rutile) in contact with an aqueous solution of pH 1–12. (Source: Reprinted with permission from Nakamura *et al*. [10]. © 2004 American Chemical Society.)

to generate terminal $(O^-)_s$ radicals, rather than being trapped at adsorbed water species to produce adsorbed $OH^•$. As discussed later, when $OH^•$ is detected in photocatalytic reactions, it should be formed by photocatalytic reduction of H_2O_2 (Eq. (1.3)).

1.2
Trapped Electron and Hole

Different from the semiconductor bulk, many electronic energy states may be formed within the band gap at the solid surface. These energy levels are capable of trapping VB holes and CB electrons. The trapped energy is considerably larger at the surface than in the bulk, indicating that it is energetically favorable for carriers to travel from the bulk to the surface [13]. At the surface, the trapping sites generally correspond to five-coordinated Ti^+ and two-coordinated O^- surface ions. When an appropriate acceptor (a scavenger), such as O_2 for electrons or methanol for holes, is adsorbed on the surface, it was suggested that the carriers should be preferentially transferred to the adsorbate rather than remain trapped at the surface sites [13].

When there are no molecules that can suffer the reaction, the existence of electrons and holes can be detected at a low temperature such as 77 K. To detect such paramagnetic species, electron spin resonance (ESR) spectroscopy is a valuable method [14, 15].

Holes and electrons could be observed by the absorption spectra just after the short pulse excitation under ambient temperature [16]. Trapped holes show that the absorption peaked at about 500 nm [17] and disappeared by the further reactions. On the other hand, trapped electrons show a broad absorption band that peaked at about 700 nm [18], which react mainly with oxygen molecules in air. Trapped electrons are so stable in the absence of O_2 that the kinetics can be explored by means of a stopped flow technique [19]. The reduction kinetics has been investigated through the electron acceptors such as O_2, H_2O_2, and NO_3^-, which are often present in photocatalytic systems. The experimental results clearly showed that the stored electrons reduce O_2 and H_2O_2 to water by multielectron transfer

processes [19]. Moreover, NO_3^- is reduced via the transfer of eight electrons evidencing the formation of ammonium ions. On the other hand, in the reduction of toxic metal ions, such as Cu(II), two-electron transfer occurs, indicating the reduction of the copper metal ion into its nontoxic metallic form.

1.3
Superoxide Radical and Hydrogen Peroxide ($O_2^{\bullet-}$ and H_2O_2)

Since photocatalysts are usually used in air, photoexcited CB electrons transfer to the oxygen in air to form superoxide radical $O_2^{\bullet-}$. The highly sensitive MIRIR technique was applied and surface intermediates of the photocatalytic O_2 reduction were directly detected. Figure 1.4 shows the proposed mechanism of the reduction of molecular oxygen at the TiO_2 surface in aqueous solutions [20]. In neutral and acidic solutions, CB electrons reduce the surface Ti^{4+} that adsorbs H_2O, and then O_2 attacks it immediately to form superperoxo TiOO$^\bullet$ as shown in path A in Figure 1.4. This superperoxo is reduced to peroxo Ti(O_2), which is equivalent to hydroperoxo TiOOH, when it is protonated (Figure 1.4). The hydroperoxo has the same structure with the hydrogen peroxide adsorbed on TiO_2 surface. On the other hand, in the alkaline solution, as shown in path B, the adsorbed O_2 receives a photogenerated CB electron to produce $O_2^{\bullet-}$. If it is not used for reactions or oxidized, the produced $O_2^{\bullet-}$ is converted to H_2O_2 by disproportionation with

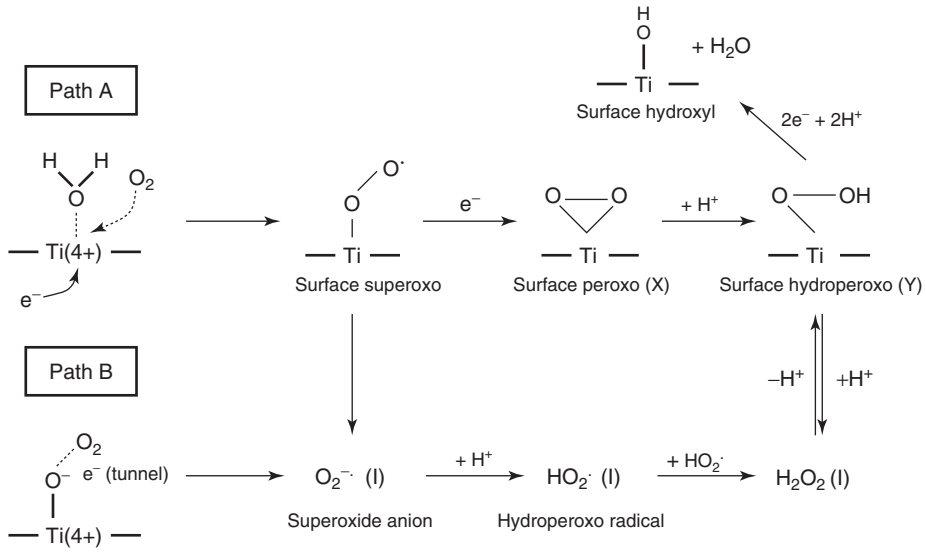

Figure 1.4 Reaction paths for the photocatalytic reduction of O_2 at the TiO_2 surface, suggested from IR measurements in neutral and acidic aqueous solutions (path A) and in an alkaline solution (path B). (Source: Reprinted with permission from Nakamura *et al*. [20]. © 2003 American Chemical Society.)

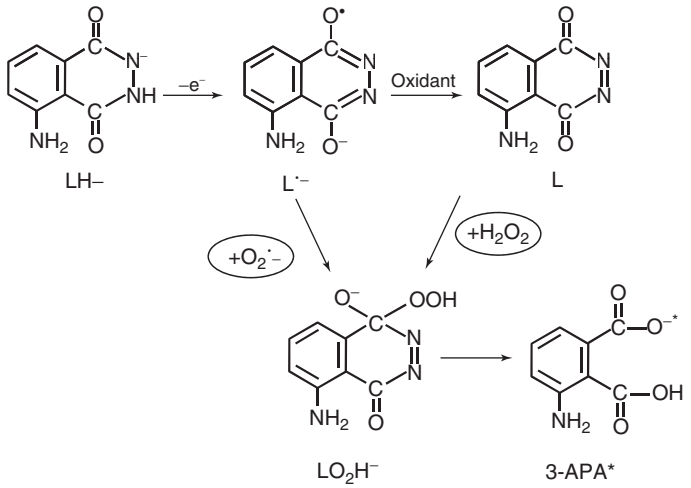

Figure 1.5 Chemiluminescence reactions for detecting $O_2^{\bullet-}$ and H_2O_2. The excited state of 3-aminophthalate (3-APA) is formed by two different reactions.

protons. Although the reaction rate for molecules having higher electron affinity is usually large, the reactivity of $O_2^{\bullet-}$ is generally weak. At pH lower than 4.8, it takes the form of $HO_2^{\bullet}$ by the protonation, whose lifetime is short owing to the rapid reaction with $O_2^{\bullet-}$ or $HO_2^{\bullet}$ to form stable H_2O_2 [7], as stated above.

Since the lifetime of $O_2^{\bullet-}$ is long in alkaline solution [21], it can be detected after stopping the irradiation. To detect $O_2^{\bullet-}$, a chemiluminescence method with luminol or luciferin analog (MCLA) has been used [22]. Figure 1.5 shows the reaction scheme for luminol chemiluminescence reactions. Luminol (LH^-) is easily oxidized in alkaline solution under air forming one-electron oxidized state ($L^{\bullet-}$), and reacts with $O_2^{\bullet-}$ to form unstable peroxide (LO_2H^-). This species releases N_2 to form the excited state of 3-aminophthalate (3-APA), which emits light at 430 nm. When L^- is oxidized further, a two-electron oxidation form of luminol (L), or a kind of diazo-naphthoquinones, is formed. It can react with H_2O_2 to form peroxides to proceed the same chemiluminescence reaction. Thus, using an oxidant, H_2O_2 could be separately detected by a luminol chemiluminescence method [23].

The decay profile of $O_2^{\bullet-}$ concentration does not obey first- or second-order kinetics, but obeys fractal-like kinetics, namely, the distribution of the distance between holes and adsorbed $O_2^{\bullet-}$ governs these decay kinetics [21]. For anatase thin film photocatalysts irradiated with very weak (1 μW cm^{-2}) UV light, the quantum yields of $O_2^{\bullet-}$ were reported to be 0.4 and 0.8 in air and water, respectively [24].

As suggested in Figure 1.2, $O_2^{\bullet-}$ may be produced by the photocatalytic oxidation of H_2O_2 (Eq. (1.4)).

$$HO_2^- + h^+ \rightarrow O_2^{\bullet-} + H^+ \tag{1.4}$$

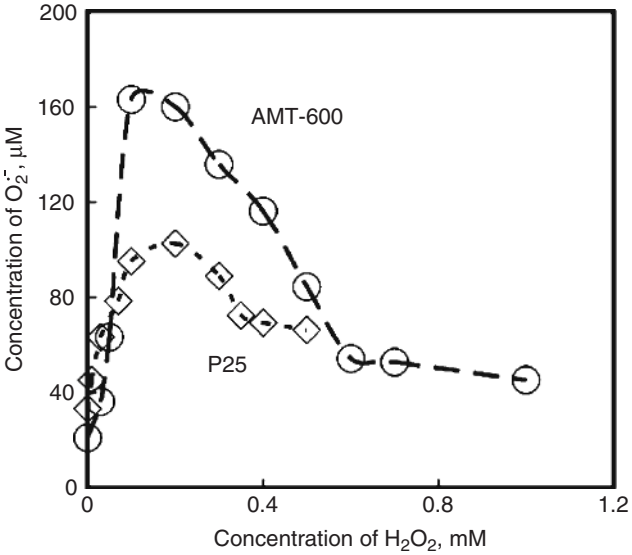

Figure 1.6 The effect of H_2O_2 on the concentration of $O_2^{\bullet-}$ measured after 100 s irradiation of the TiO_2 suspension of AMT-600 (TAYCA Corp.) and P25 (Nippon Aerosil Co., Ltd).

Figure 1.6 shows the amount of $O_2^{\bullet-}$ formed after 10 s in the presence of H_2O_2 of various concentrations. Increase in $O_2^{\bullet-}$ was observed with a small amount of H_2O_2, indicating the oxidation of H_2O_2 with photogenerated hole h^+ (Eq. (1.4)) or the increase in the reduction of O_2 owing to the suppression of photogenerated e^- from the recombination. When the amount of H_2O_2 was larger than 0.2 mmol l^{-1}, the formation of $O_2^{\bullet-}$ decreased, indicating that the adsorption of H_2O_2 on the whole surface blocks the access of O_2, which would increase the electron–hole recombination rate.

1.4 Hydroxyl Radical (OH•)

Although OH• has been usually recognized as the most important active species of the photocatalytic oxidation, recent reports confirmed that the contribution of OH• in the photocatalytic oxidation process is not usually dominant [6]. It should be emphasized that OH• has been referred too easily to be involved in the oxidation mechanism of photocatalytic reactions.

Several methods to detect OH• in photocatalytic reactions have been reported. Usually, the spin trapping reagents, such as DMPO (5,5-dimethyl-1-pyrroline-*N*-oxide), have been used to detect OH radicals (Figure 1.7a). However, it is not a molecule stable enough in aerated aqueous solutions and can be easily oxidized. In many reports, the possibility of the other reactions for DMPO than the OH radical adduction has not been anticipated. Based on the detailed study in [25],

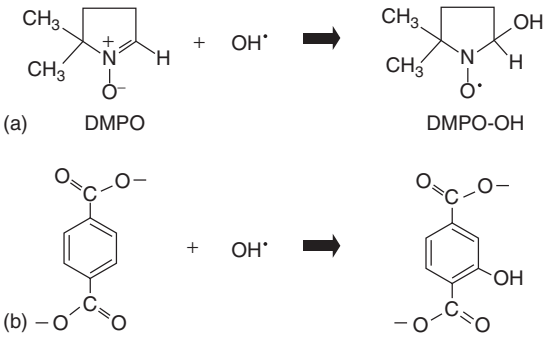

Figure 1.7 (a) The spin trapping reaction for $OH^{\bullet}$ with DMPO. (b) The reaction of terephthalic acid with $OH^{\bullet}$ forming fluorescent 2-hydroxy terephthalate.

it was indicated that the amount of radical adduct in the photocatalytic reaction was increased with DMPO concentration and that no saturation was observed, whereas $OH^{\bullet}$ formed by photolysis of H_2O_2 could be trapped by excess amount of DMPO. This means that the OH radical adduct DMPO–$OH^{\bullet}$ was formed by the photocatalytic reaction of DMPO itself and not through OH radicals. Thus, spin trapping experiments for detecting $OH^{\bullet}$ must be carefully performed to prove the presence of $OH^{\bullet}$ [25, 26].

A fluorescence probing method, based on the reaction of $OH^{\bullet}$ with stable molecules seems more suitable than those with unstable spin trapping regents. In the field of radiation chemistry, the reactions of $OH^{\bullet}$ with terephthalic acid (TA) and coumarin have been used because these products show strong fluorescence aiding in sensitive detection [27]. Therefore, this method has been adopted to detect $OH^{\bullet}$ in photocatalytic reactions in aqueous suspension systems [28, 29]. The quantum yield of $OH^{\bullet}$ in TiO_2 aqueous suspension was on the order of 10^{-5} [30]. Kinetic analysis for the formation rates of the $OH^{\bullet}$ adduct (DMPO–$OH^{\bullet}$) along with the competitive adsorption of phosphate showed that, at a pH = 4.25, phthalic acid that was adsorbed on TiO_2 surface was oxidized directly by VB holes, with a quantum yield of 0.08 [31]. This high quantum yield could be attributed to the direct oxidation of adsorbed TA with VB holes.

Since radicals can be sensitively analyzed with ESR, nitroxide radical (3-carboxy-2,2,5,5-tetramethyl-1-pyrrolidine-1-oxy) has been used as a probe to detect OH radicals [32]. The quantum efficiencies of $OH^{\bullet}$ for several TiO_2 photocatalysts were measured by the TA fluorescence method (Figure 1.7b) and compared with those obtained with the spin-trap and spin-probe ESR methods stated above [29]. The $OH^{\bullet}$ yields measured by the TA fluorescence method were smaller by a factor of about 100, showing no correlation with those obtained by the DMPO spin trapping and the TA spin probing methods. Although the formation of $OH^{\bullet}$ has been reported mainly using the spin trapping method, the contribution of the free $OH^{\bullet}$ may be very small when the reactant is readily oxidized. Thus, the $OH^{\bullet}$ should be distinguished from that generated by the trapped holes in photocatalytic reactions.

OH• was expected to be directly detected by means of ESR spectroscopy at low temperature. However, actually the OH• was not detected by ESR spectroscopy at 77 K, but only trapped holes were detected for hydrated TiO_2 particles [33]. Under hydrated conditions, when the frozen trapped holes were partly melted, they oxidized the adsorbed molecules [33]. Thus, the involvement of OH• in the oxidation process was not proved by direct detection with ESR.

Another definite method to confirm the presence of OH• is the observation of the optical absorption spectrum in gas phase. By scanning the excitation wavelength (282–284 nm) and monitoring the fluorescence at 310 nm, the spectrum could be identified as the absorption lines of OH•. This highly sensitive and selective technique is called as the laser-induced fluorescence (LIF) method. Using this method, the first direct observation of the presence of OH• in TiO_2 photocatalytic systems was reported [34]. The quantum yield of OH• calculated from the LIF intensity was about 5×10^{-5}. When the O_2 gas of low partial pressures was flowed, the formation of OH• was clearly enhanced. Since the addition of H_2O_2 on the TiO_2 surface increased the LIF intensity, H_2O_2 molecules were also considered to form by the reduction reactions of O_2. The addition of methanol (a scavenger of hole) decreased significantly the LIF signal intensity, suggesting the formation of H_2O_2 by the oxidation of surface OH groups by holes. This mechanism of OH• formation is illustrated in Figure 1.8 [34]. With a similar reaction system, the formation and diffusion of H_2O_2 have been reported using the LIF method [35]. Consequently, it was proved that OH radicals are mainly formed by the reduction of H_2O_2, which is formed by the two-electron reduction of O_2 and/or two-electron oxidation of H_2O.

Using a molecular fluorescence marker, the diffusion of OH• from TiO_2 surface during UV irradiation has been verified [36]. The detected amount of OH• decreased with decreasing the concentration of oxygen, that is, at $[O_2] = 0.2$ vol%, no significant amount of OH• was detected. This result indicates that the OH• formation is very sensitive to the oxygen concentration, and the reduction process of oxygen, which results in the formation of $O_2^{\bullet -}$ leading to H_2O_2, is a key process in the formation of OH•.

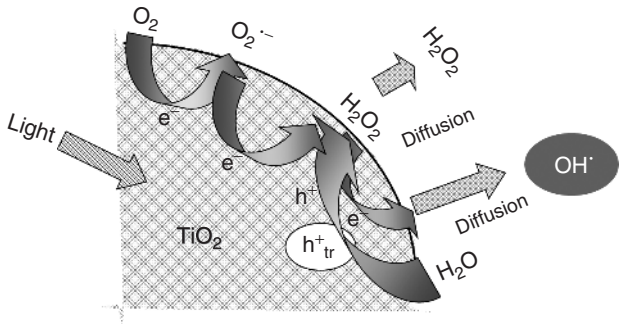

Figure 1.8 A plausible reaction scheme for the OH radical formation on the irradiated TiO_2 surface.

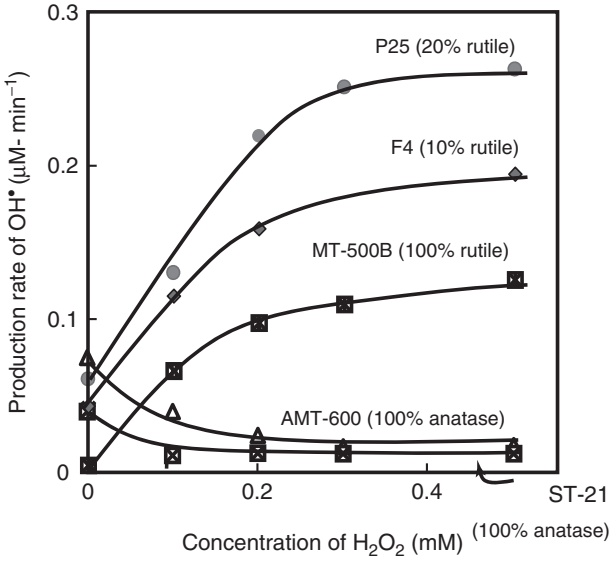

Figure 1.9 The formation rates of $OH^{\bullet}$ measured by a fluorescence probe method plotted for several TiO_2 photocatalysts as a function of the concentration of H_2O_2. (Source: Reprinted with permission from Hirakawa *et al*. [37]. © 2007 Elsevier.)

The effect of H_2O_2 addition on the rate of $OH^{\bullet}$ formation in aqueous suspension systems was measured for various TiO_2 [37]. As shown in Figure 1.9, the $OH^{\bullet}$ formation rates were increased with the addition of H_2O_2 for P25 (Nippon Aerosil Co, Ltd) and F4 (Showa Titanium Co., Ltd) TiO_2, which are rutile-containing anatase, and for rutile TiO_2 (MT-500B, TAYCA Corp.). The quite opposite tendency was observed for AMT-600 (TAYCA Corp.) and ST-21 (Ishihara Sangyo Co., Ltd), which consist of 100% anatase TiO_2, where the $OH^{\bullet}$ formation rate decreased on H_2O_2 addition. The increase of $OH^{\bullet}$ is attributable to the photocatalytic reduction of H_2O_2 (Eq. (1.3)). Since the rutile-containing anatase increased the $OH^{\bullet}$ generation, the structure of H_2O_2 adsorbed on the rutile TiO_2 surface is likely preferable to produce $OH^{\bullet}$.

1.5
Singlet Molecular Oxygen ($^1O_2$)

To explain the formation of singlet oxygen, the disproportionation of $O_2^{\bullet -}$ was proposed through the intermediate formation of $HO_2^{\bullet}$ as shown by Eq. (1.5) [38]. Since the energy difference of $HO_2^{\bullet} \rightarrow O_2$ from $HO_2^{\bullet} \rightarrow H_2O_2$ at a pH = 0 is calculated to be +1.49 V from Figure 1.2, O_2 may be excited to $^1O_2$. But, it becomes 0.53 V at pH = 14, which is smaller than the excitation energy of 0.98 eV (or 1270 nm in wavelength).

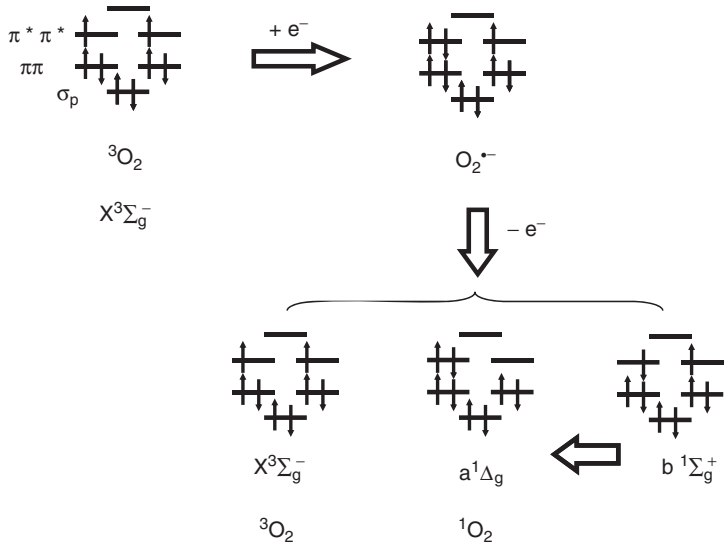

Figure 1.10 The spin states in the process of singlet molecular oxygen formation via the oxidation of O_2^-.

Alternatively, the oxidation of $O_2^{\bullet-}$ as indicated by Eq. (1.6) has been proposed as the formation mechanism [39]. Since $O_2^{\bullet-}$ is formed by the electron transfer of photoexcited CB electrons at the surface, it may be easily oxidized.

$$2HO_2^{\bullet} \rightarrow (HOOOOH) \rightarrow {}^1O_2 + H_2O_2 \tag{1.5}$$

$$O_2^{\bullet-} + h^+ \rightarrow {}^1O_2 \tag{1.6}$$

Figure 1.10 shows the plausible pathways for the consecutive reduction and oxidation of O_2. Since three electrons in the π^* state of $O_2^{\bullet-}$ cannot be distinguished from one another, three electronic states may be produced depending on the removed electron. These are $^3\Sigma_g^-$, $^1\Delta_g$, and $^1\Sigma_g^+$ states in the order from the lower energy. The last two states are electronic excited states of molecular oxygen and named as *singlet oxygen*. The lifetime of the $^1\Sigma_g^+$ state is very short and immediately transfers to the $^1\Delta_g$ state of singlet molecular oxygen ($^1O_2$). The lifetime of the $^1\Delta_g$ state depends largely on its environment, ranging from a few microseconds in H_2O to a few milliseconds in air.

Among the detection methods to verify the formation of $^1O_2$, one of the most established methods is to observe the phosphorescence at 1270 nm, which is the radiative transition from the $a^1\Delta_g$ state to the $X^3\Sigma_g^-$ state of molecular oxygen. The phosphorescence at 1270 nm has been detected in a TiO_2 aqueous suspension system [39]. Quantum yields for $^1O_2$ generation measured for 10 commercial TiO_2 photocatalysts in air ranged from 0.12 to 0.38, while the lifetimes ranged from 2.0 to 2.5 μs [40]. The production and decay of $^1O_2$ in TiO_2 photocatalysis were investigated by monitoring the phosphorescence under various reaction

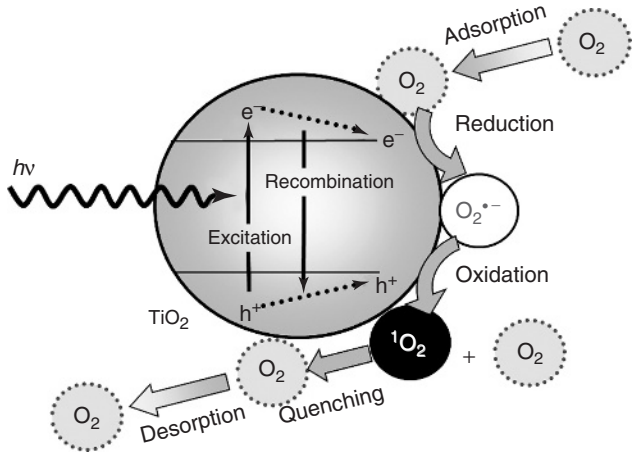

Figure 1.11 Photocatalytic processes of molecular oxygen on the TiO_2 surface. (Source: Reprinted with permission from Daimon *et al.* [40]. © 2007 American Chemical Society.)

conditions. The comparison among the effects of additives such as KBr, KSCN, KI, and H_2O_2 on the formation of $^1O_2$ and $O_2^{\bullet-}$ suggested that $^1O_2$ should be formed by the electron transfer mechanism (Eq. (1.6)), as illustrated in Figure 1.11. The formation of $^1O_2$ decreased at pH $<$ 5 and pH $>$ 11, indicating that the intermediate $O_2^{\bullet-}$ is stabilized at the terminal OH site of the TiO_2 surface in this pH range. Eighteen commercially available TiO_2 photocatalysts were compared on the formation of $^1O_2$ and $O_2^{\bullet-}$ in an aqueous suspension system. The formation of $^1O_2$ was increased with decreasing the size of TiO_2 particles, indicating that a large specific surface area causes a higher possibility of reduction producing $O_2^{\bullet-}$ and therefore, a large amount of $^1O_2$ is formed. The difference in the crystal phase (rutile and anatase) does not seem to affect the formation of $^1O_2$ [41].

Singlet oxygen is known to be reactive with some organic compounds such as olefines and amines. Therefore, in the presence of four kinds of organic molecules, methionine, pyrrole, collagen, and folic acid (pteroyl-L-glutamic acid), the decay of $^1O_2$ was measured [42]. Figure 1.12a represents the total decay of $^1O_2$, and Figure 1.12b shows the partial decay obtained after subtraction of the intrinsic exponential decay. The observed decay rates of $^1O_2$ with these organic molecules are significantly higher than those expected from the bimolecular rate constant reported for the reaction in homogeneous solution. By assuming pseudo-first-order reaction, the virtual concentrations of the reactant are in the vicinity of 0.01 mol l^{-1}. Since the concentration of the solution used in the experiments was 0.01 mmol l^{-1}, the organic reactants must be concentrated at the surface of TiO_2 by adsorption. These observations suggest that the reactant molecules should be adsorbed on the TiO_2 surface [42]. Although the 40% of $^1O_2$ was deactivated with folic acid, this deactivation process includes thermal deactivation besides the chemical reactions.

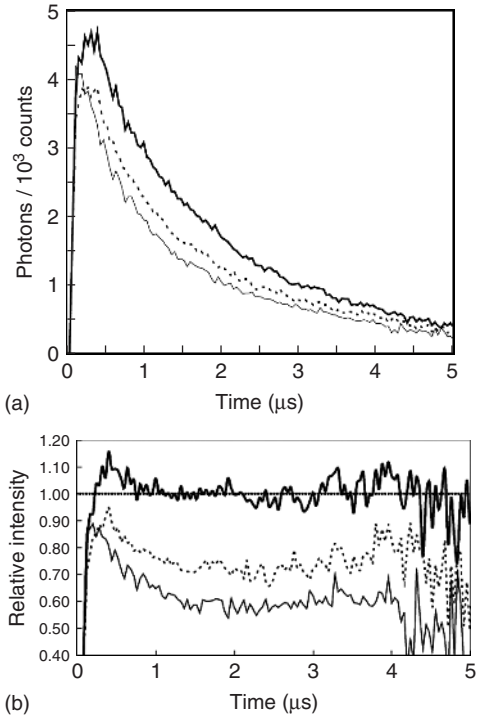

Figure 1.12 The time dependence of phosphorescence intensity for singlet molecular oxygen monitored at 1250 nm after the pulsed excitation on P25 TiO_2 aqueous suspension. Without additives (heavy line), with methionine (dashed line), and folic acid (fine line). (a) Original observation of emission intensity as the time profile. (b) The partial decay obtained after subtraction of the intrinsic exponential decay showing the fast decay by the reaction. (Source: Reprinted from Daimon et al. [42]. copyright 2008 Electrochemical Society of Japan.)

1.6 Reaction Mechanisms for Bare TiO_2

There are many reaction pathways in any photocatalytic reaction system. Whenever a certain pathway in question is discussed, the other pathways should also be considered simultaneously. To detect $^1O_2$ in the reaction system, sterically hindered cyclic amines, such as HTMP (4-hydroxy-2,2,6,6-tetramethylpiperidine), have been used as probe molecules [43]. Such amines are converted to the corresponding stable aminoxyl radical (nitroxide radical) which can be sensitively detected by ESR spectroscopy. In the case of HTMP, TEMPOL radical (4-hydroxy-2,2,6,6-tetramethyl piperidine 1-oxyl) is formed as a result of a photocatalytic reaction in a TiO_2 aqueous suspension. The time profiles of the radical formation and the effect of additives, such as SCN^-, I^-, methanol, and H_2O_2, on the initial formation rates were measured in order to elucidate the photocatalytic reaction mechanism for HTMP [44]. By assuming possible key reactants for the oxidation as shown in Figure 1.13,

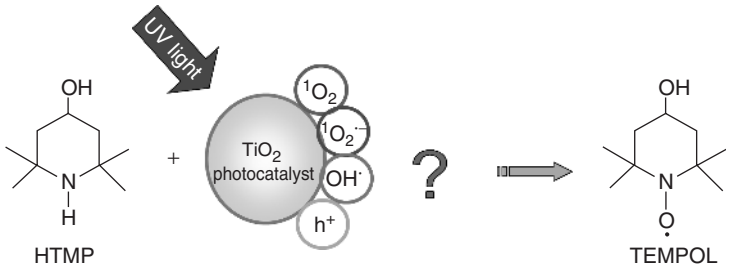

Figure 1.13 Key reactants considered for the kinetic analysis of the photocatalytic formation of nitroxide radicals.

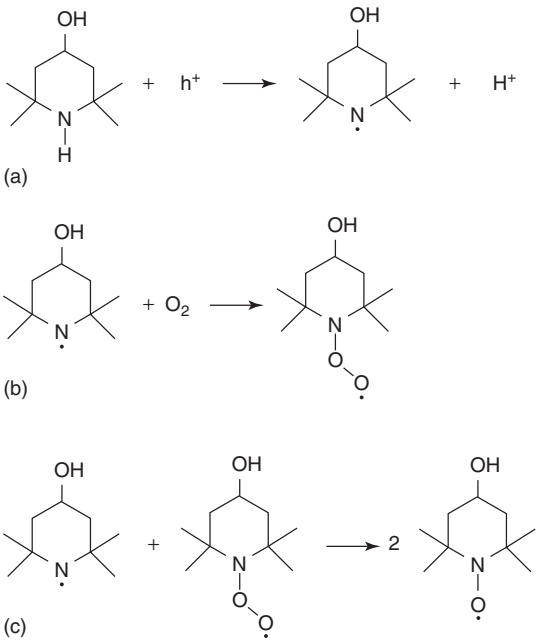

Figure 1.14 (a–c) Plausible photocatalytic reaction processes of sterically hindered cyclic amine.

the kinetics was analyzed to elucidate the reaction process. The experimental observations indicated that the direct photocatalytic oxidation of HTMP followed by reaction with O_2 is the dominant process in the formation of TEMPOL radicals (Figure 1.14). The possibility of the other processes, involving reactions with $^1O_2$, $O_2^{\bullet-}$, and $OH^{\bullet}$, was excluded from the reaction mechanism.

As stated above, $OH^{\bullet}$ is not produced through a main oxidation process even in the absence of organic compounds. However, in most of the research papers on photocatalysis published so far, $OH^{\bullet}$ has often been regarded to be involved in the actual oxidation mechanism of photocatalytic reactions. However, actually the primary reaction pathway for the oxidation is the direct reaction at the surface

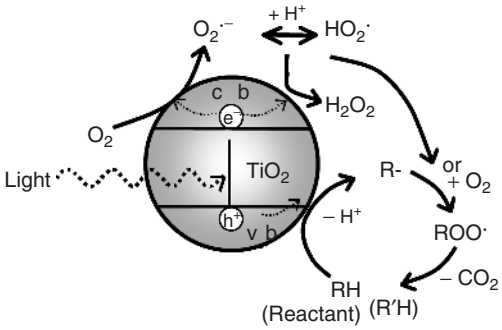

Figure 1.15 General reaction processes for the photocatalytic oxidation of organic molecules.

of TiO_2 with VB holes or trapped holes. Since it is generally known that the photocatalytic oxidation of organic compounds is accelerated by oxygen [45], the produced radical may react with the reduction products of O_2, namely, $O_2^{\bullet -}$ and H_2O_2. But the O_2 in air may directly react with the radical produced by the photocatalytic oxidation, because auto-oxidation, a kind of chain reaction with O_2 starting from organic free radicals, is well known [46]. The consumption of O_2 at the oxidation site of the photocatalyst has been suggested from the experiment of electrochemical probe reactions at the surface of illuminated TiO_2 photoelectrode [47]; the generalized reaction mechanism of the photocatalytic oxidation of organic molecules (RH) is illustrated in Figure 1.15. RH will degrade by losing one carbon atom by releasing CO_2, but the intermediates may be aldehyde R′CHO or carboxylate $R'COO^-$.

1.7 Reaction Mechanisms of Visible-Light-Responsive Photocatalysts

As promising practical applications of photocatalysts, the utilization of visible light has been promoted. Figure 1.16 shows the energy levels of some visible-light-responsive photocatalysts. Since the energy level of VB for metal oxides is governed by that of the O-2p orbital, a narrow-band-gap metal oxide semiconductor, such as WO_3, possesses CB energy lower than that of TiO_2. Since the one-electron reduction potential of O_2 is very close to that of the CB of TiO_2, as shown in Figure 1.2, WO_3 is unable to form $O_2^{\bullet -}$, as shown in Figure 1.16a. In this case, using a promoter such as deposited Pt [48], electrons could be stored to enable two-electron reduction of O_2 to H_2O_2. Doping to produce the mid-gap level has been proposed as the other visible-light-responsive photocatalysis. Since the energy level of VB has sufficient oxidation ability, shifting the VB by doping the N or S anion has been attempted (Figure 1.16b). In this case, photogenerated holes produced on the donor level are expected to have oxidation ability similar to that of bare TiO_2 [23]. As shown in Figure 1.16c, photocatalysts of the photosensitization type were

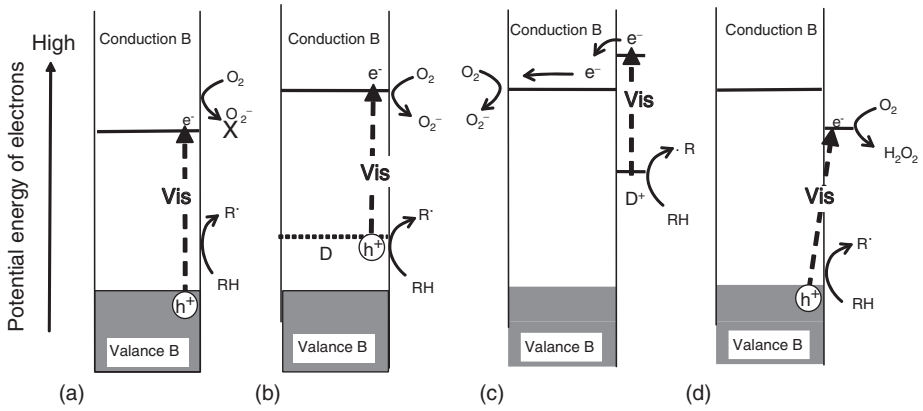

Figure 1.16 Classification of visible-light-responsive photocatalysts by the mechanism of reaction. (a) Narrow-band-gap semiconductor such as WO_3, (b) anion-doped TiO_2 such as nitrogen-doped TiO_2, (c) sensitizer-deposited TiO_2 such as $PtCl_6^{2-}$-deposited TiO_2, and (d) interfacial-charge-transfer-type TiO_2 such as Cu(II)-grafted TiO_2.

also proposed. The deposited compound absorbs the visible light and transfers the excited electron to produce a cation radical, which can oxidize organic pollutant molecules. In this case, enough oxidation power with good stability is required as an oxidized sensitizer [49]. Recently, interfacial charge transfer (IFCT)-type absorption originating from the excitation of VB electrons to deposited (or grafted) metal ions has been proposed (Figure 1.16d). In this case, if the deposited compound has a catalytic ability of O_2 reduction, the efficiency is expected to be increased [50].

The observation of active species such as $O_2^{\bullet-}$ and H_2O_2 is inevitable to confirm the reaction mechanism proposed. Figure 1.17 shows the formation of $O_2^{\bullet-}$ as a function of irradiation time of 442 nm light for several visible-light-responsive photocatalysts. For $PtCl_6^{2-}$-modified TiO_2, a large amount of $O_2^{\bullet-}$ was observed immediately after the excitation, in concord with the electron transfer to the CB (Figure 1.16c). On the other hand, Fe-complex-deposited TiO_2 generated a small amount of $O_2^{\bullet-}$ probably because the excitation takes place from VB to Fe ions at the surface (Figure 1.16d). For the S-doped TiO_2, the amount of $O_2^{\bullet-}$ increased as the irradiation period increased, and reached a steady value in 30 s, while for the N-doped TiO_2, it gradually increased up to about 180 s. In a control experiment, P25 TiO_2 did not produce $O_2^{\bullet-}$ by visible-light irradiation at 442 nm, whereas on UV irradiation at 325 nm (with the similar number of photons to 442 nm) for 180 s, 20 nmol l^{-1} of $O_2^{\bullet-}$ was produced, indicating that the steady-state concentrations of $O_2^{\bullet-}$ for the N- and S-doped TiO_2 are higher than those for the undoped TiO_2 (P25) [23].

Figure 1.18 schematically shows the dominant reaction processes in the absence of organic substrates, which are deduced from the observation of $O_2^{\bullet-}$ and H_2O_2 [23]. The S-doped TiO_2 surpassed the N-doped TiO_2 in the production of $O_2^{\bullet-}$, while the N-doped TiO_2 surpassed the S-doped TiO_2 in the production of H_2O_2. Since $O_2^{\bullet-}$ decays obeying the second-order kinetics, H_2O_2 is mainly produced from the disproportionation of $O_2^{\bullet-}$. The production of $O_2^{\bullet-}$ decreased by adding

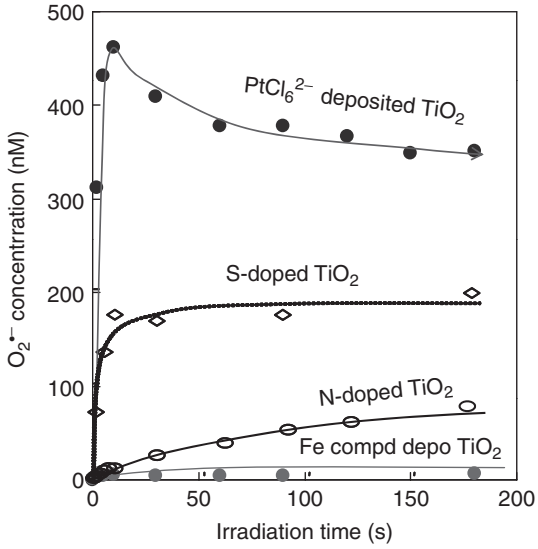

Figure 1.17 The concentration of $O_2^{\bullet-}$ produced in the suspension (15 mg per 3.5 ml) of the modified TiO_2 photocatalyst powders as a function of the irradiation time of 442 nm light.

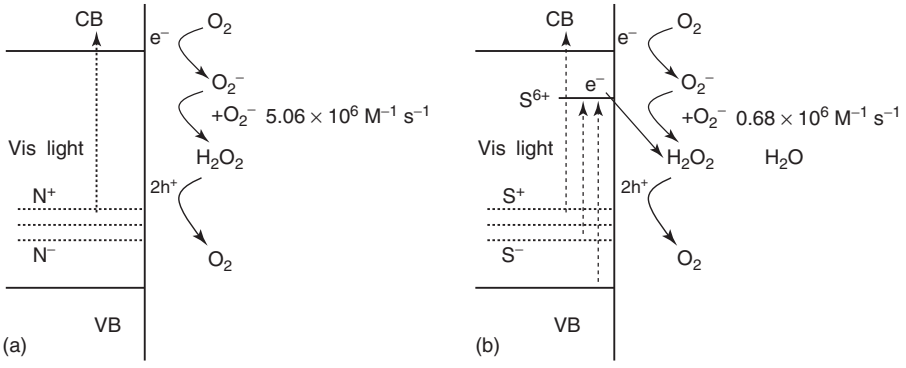

Figure 1.18 Proposed photocatalytic reaction processes of $O_2^{\bullet-}$ and H_2O_2 on the N- and S-doped TiO_2 in the absence of organic substrates. (a) The N-doped TiO_2 selectively produces H_2O_2, while (b) the S-doped TiO_2 produces $O_2^{\bullet-}$ and reduces H_2O_2 to water. (Source: Reprinted with permission from Hirakawa *et al.* [18]. © 2008 American Chemical Society.)

H_2O_2 to both N- and S-doped TiO_2. Therefore, H_2O_2 would not be oxidized in both N- and S-doped TiO_2, which is in prominent contrast to the undoped TiO_2 (P25). The H_2O_2 produced by the S-doped TiO_2 might be quickly reduced to H_2O via some intermediate states; the reactive oxygen species produced by the reduction of H_2O_2 may play an important role in the decomposition of organic molecules, and the S-doped TiO_2 may surpass N-doped TiO_2 in this ability.

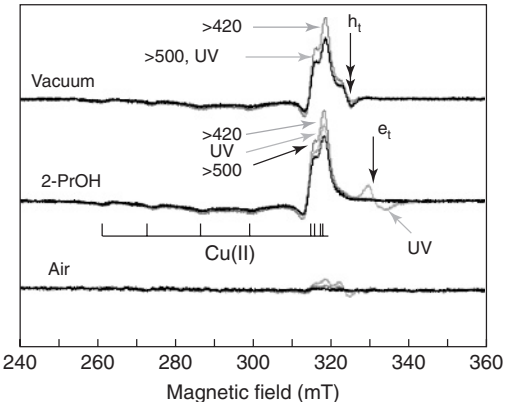

Figure 1.19 ESR difference spectra for Cu(II)/TiO_2 measured under vacuum, with 2-propanol, and air showing the effects of light irradiation at the wavelengths around 360 nm, longer than 420 and 500 nm, respectively. (Source: Reprinted with permission from Nosaka *et al*. [51]. © 2011 American Chemical Society.)

For visible-light-responsive photocatalysts of IFCT type with metal ions (Figure 1.16d), ESR spectroscopy could be utilized to analyze the state of the metal ions. Figure 1.19 shows the difference in the ESR spectra caused by light irradiation for Cu(II)-deposited TiO_2 [51]. The decrease of the large signal, characterized by a hyperfine splitting by Cu nuclear spin, indicates the decrease of Cu^{2+} ions on visible-light irradiation under vacuum. In the presence of air, the signal of Cu^{2+} did not change with the irradiation, indicating the reduced Cu^{+} reacts with O_2 to reproduce Cu^{2+}. This fact and the observation of $O_2^{\bullet-}$ formation clearly supported the IFCT mechanism for the Cu(II)-deposited TiO_2 photocatalysts. For WO_3 photocatalyst, which is classified to Figure 1.16a, the formation of $O_2^{\bullet-}$ was not observed on 442 nm excitation [51]. When it was grafted with Cu(II), the reduction of Cu^{2+} in ESR spectrum and the formation of H_2O_2 were observed. The formation of H_2O_2 indicated the function of Cu(II) as a promoter for two-electron reduction of O_2. The reaction mechanisms of Cu(II)/TiO_2 and Cu(II)/WO_3 photocatalysts are illustrated in Figure 1.20 [51]. Thus, the reaction pathways for different types of visible-light-responsive photocatalysts could be confirmed by the detection of primarily produced active species.

1.8 Conclusion

In order to explore the reaction mechanism of bare TiO_2 and TiO_2 photocatalysts modified for visible-light response, the detection and the behaviors of key species, such as trapped electrons, superoxide radical ($O_2^{\bullet-}$), hydroxyl radical ($OH^{\bullet}$), hydrogen peroxide (H_2O_2), and singlet oxygen ($^1O_2$), were discussed. Trapped electrons, which have been analyzed at 77 K with ESR spectroscopy, are so stable in the

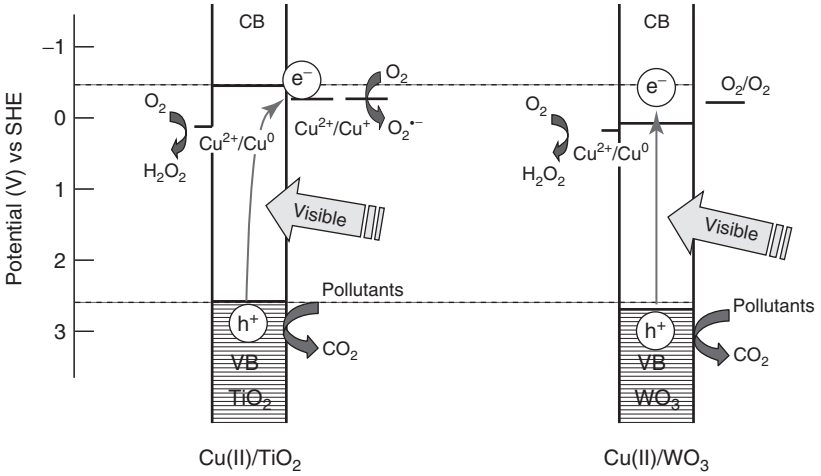

Figure 1.20 Energy diagrams of Cu(II)-grafted TiO_2 (rutile) and WO_3 photocatalysts at pH 7 showing the photocatalytic reaction mechanisms under visible-light irradiation. (Source: Reprinted with permission from Nosaka *et al.* [51]. © 2011 American Chemical Society.)

absence of O_2 that the kinetics can be investigated by means of a stopped flow technique. O_2 in air receives a photogenerated CB electron or trapped electron to produce $O_2^{\bullet-}$, which is converted to more stable H_2O_2. Since the rutile-containing anatase increased the $OH^\bullet$ generation, the structure of H_2O_2 adsorbed on the rutile TiO_2 surface might be preferable to produce $OH^\bullet$. Only partial decay of $^1O_2$ with folic acid, which is a well-known reactant of $^1O_2$, was observed, suggesting that the role of $^1O_2$ in photocatalysis is not major. A general reaction pathway for bare TiO_2, in which organic compounds are oxidized directly to form organic radicals followed by the auto-oxidation with O_2 and release of CO_2, has been proposed. Furthermore, for some types of visible-light-responsive photocatalysts, the reaction mechanisms were compared by the detection of the primarily produced key species and the reaction pathways could be proposed.

References

1. Fujishima, A., Zhang, X., and Tryk, D. A. (2008) TiO_2 Photocatalysis and related surface phenomena, *Surf. Sci. Rep.* **63**, 515–582.
2. Kaneko, M., Ohkura, I., (eds) (2002) *Photocatalysis*, Kodansha-Springer, Ltd, Tokyo.
3. Zhang, H., Chen, G., and Bahnemann, D.W. (2009) Photoelectrocatalytic materials for environmental applications, *J. Mater. Chem.* **19**, 5089–5121.
4. Y. Paz, (2010) Composite titanium dioxide photocatalysts and the ''adsorb & shuttle'' approach: a review, *Solid State Phenom.*, **162**, 135–162.
5. P. Pichat (2010), Some views about indoor air photocatalytic treatment using TiO_2: conceptualization of humidity effects, active oxygen species, problem of C_1–C_3 carbonyl pollutants, *Appl. Catal., B* **99** 428–434.
6. Henderson, M. A. (2011) A surface science perspective on TiO_2

photocatalysis, *Surf. Sci. Rep.* **66**, 185–297.
7. Bielski, B. H. J., Cabelli, D. E., and Arudi, R. L. (1985) Reactivity of HO_2/O_2^- radicals in aqueous solution, *J. Phys. Chem. Ref. Data*, **14**(4), 1041–1100.
8. Bard, A. J., Parsons, R., and Jordan, J., (eds) (1985) *Standard Potentials in Aqueous Solution*, Marcel Dekker, New York.
9. Minero, C., Mariella, G., Maurino, V., and Pelizzetti, E. (2000), Photocatalytic transformation of organic compounds in the presence of inorganic anions. 1. Hydroxyl-mediated and direct electron-transfer reactions of phenol on a titanium dioxide-fluoride system, *Langmuir*, **16**, 2632–2641.
10. Nakamura, R., and Nakato, Y. (2004) Primary intermediates of oxygen photoevolution reaction on TiO_2 (rutile) particles, revealed by in situ FTIR absorption and photoluminescence measurements, *J. Am. Chem. Soc.* **126**(4), 1290–1298.
11. Muryn, C. A., Hardman, P. J., Crouch, J. J., Raiker, G. N., Thornton, G. D., and Law, S. L. (1991) Step and point defect effects on TiO_2(100) reactivity, *Surf. Sci.*, **251–252**, 747–752.
12. Salvador, P. (2007) On the nature of photogenerated radical species active in the oxidative degradation of dissolved pollutants with TiO_2 aqueous suspensions: a revision in the light of the electronic structure of adsorbed water, *J. Phys. Chem. C*, **111**(45), 17038–17043.
13. Valentin, C. D. and Selloni, A. (2011) Bulk and surface polarons in photoexcited anatase TiO_2, *J. Phys. Chem. Lett.*, **2**, 2223–2228.
14. Formenti, M., Juillet, F., Meriaudeau, P., and Teichner, S. J. (1971) Heterogeneous photocatalysis for partial oxidation of paraffins. *Chem. Technol.*, **1**, 680–686.
15. Nakaoka, Y., and Nosaka, Y. (1997) ESR investigation into the effects of heat treatment and crystal structure on radicals produced over irradiated TiO_2 powder. *J. Photochem. Photobiol., A*, **110**, 299–307.
16. Murakami, Y., Nishino, J., Mesaki, T., and Nosaka, Y. (2011) Femtosecond diffuse reflectance spectroscopy of various commercially available TiO_2 powders, *Spectrosc. Lett.*, **44**(2) 88–94.
17. Yang, X., and Tamai, N. (2001) How fast is interfacial hole transfer? *In situ* monitoring of carrier dynamics in anatase TiO_2 nanoparticles by femtosecond laser spectroscopy, *Phys. Chem. Chem. Phys.* **3**, 3393–3398.
18. Kamat, P. V., Bedja, I., and Hotchandani, S. (1994) Photoinduced charge transfer between carbon and semiconductor clusters. one-electron reduction of C_{60} in colloidal TiO_2 semiconductor suspensions. *J. Phys. Chem.* **98** (37), 9137–9142.
19. Mohamed, H., Mendive, C. B., Dillert, R., and Bahnemann, D. W. (2011) Kinetic and mechanistic investigations of multielectron transfer reactions induced by stored electrons in TiO_2 nanoparticles: a stopped flow study, *J. Phys. Chem. A*, **115**, 2139–2147.
20. Nakamura, R., Imanishi, A., Murakoshi, K., and Nakato, Y. (2003) In situ FTIR studies of primary intermediates of photocatalytic reactions on nanocrystalline TiO_2 films in contact with aqueous solutions, *J. Am. Chem. Soc.* **125**(24), 7443–7450.
21. Hirakawa, T., and Nosaka, Y. (2002) Properties of $\cdot O_2^-$ and ·OH formed in TiO_2 aqueous suspensions by photocatalytic reaction and the influence of H_2O_2 and some ions, *Langmuir*, **18**(8), 3247–3254.
22. Nosaka, Y., Yamashita, Y., and Fukuyama, H. (1997) Application of chemiluminescent probe to monitoring superoxide radicals and hydrogen peroxide in TiO_2 photocatalysis, *J. Phys. Chem. B*, **101**(30), 5822–5827.
23. Hirakawa, T., and Nosaka, Y. (2008) Selective production of superoxide ions and hydrogen peroxide over nitrogen- and sulfur-doped TiO_2 photocatalysts with visible light in aqueous suspension systems, *J. Phys. Chem. C*, **112**(40), 15818–15823.
24. Ishibashi, K., Fujishima, A., Watanabe, T., and Hashimoto, K. (2000) Generation and deactivation processes of superoxide formed on TiO_2 film illuminated by very weak UV light in air

or water, *J. Phys. Chem. B*, **104**(20), 4934–4938.
25. Grela, M. A., Coronel, M. E. J., and Colussi, A. J. (1996) Quantitative spin-trapping studies of weakly illuminated titanium dioxide sols. Implications for the mechanism of photocatalysis, *J. Phys. Chem.* **100**(42), 16940–16946.
26. Brezova, V., Stasko, A., Biskupic, S., Blazkova, A., and Havlinova, B. (1993) Kinetics of hydroxyl radical spin trapping in photoactivated homogeneous (H_2O_2) and heterogeneous (TiO_2, O_2) aqueous systems. *J. Phys. Chem.*, **98**, 8977–8984.
27. Matthews, R. W. (1980) The radiation chemistry of the terephthalic dosimeter, *Radiat. Res.*, **83**(1), 27–41.
28. Ishibashi, K., Fujishima, A., Watanabe, T., and Hashimoto, K. (2000) Detection of active oxidative species in TiO_2 photocatalysis using the fluorescence technique. *Electrochem. Commun.* **2**, 207–210.
29. Nosaka, Y., Komori, S., Yawata, K., Hirakawa, T., and Nosaka, A. Y. (2003) Photocatalytic OH radical formation in TiO_2 aqueous suspension studied by several detection methods, *Phys. Chem. Chem. Phys.* **5**, 4731–4735.
30. Ishibashi, K., Fujishima, A., Watanabe, T., and Hashimoto, K. (2000) Quantum yields of active oxidative species formed on TiO_2 photocatalyst, *J. Photochem. Photobiol., A*, **134**, 139–142.
31. Taborda, A. V., Brusa, M. A., and Grela, M. A. (2001) Photocatalytic degradation of phthalic acid on TiO_2 nanoparticles, *Appl. Catal., A*, **208**, 419–426.
32. Schwarz, P. F., Turro, N. J., Bossmann, S. H., Braun, A. M., Wahab, A.-M. A. A., and Durr, H. (1997) A new method to determine the generation of hydroxyl radicals in illuminated TiO_2 suspensions, *J. Phys. Chem. B*, **101**(36), 7127–7134.
33. Micic, O. I., Zhang, Y., Cromack, K. R., Trifunac, A. D., and Thurnauer M. C. (1993) Trapped holes on TiO_2 colloids studied by electron paramagnetic resonance, *J. Phys. Chem.*, **97**(28), 7277–7283.
34. Murakami, Y., Endo, K., Ohta, I., Nosaka, A. Y., and Nosaka, Y. (2007) Can OH radicals diffuse from the UV-irradiated photocatalytic TiO_2 surfaces? laser-induced-fluorescence study, *J. Phys. Chem. C*, **111**(30), 11339–11346.
35. Thiebaud, J., Thevenet, F., and Fittschen, C. (2010) OH radicals and H_2O_2 molecules in the gas phase near to TiO_2 surfaces, *J. Phys. Chem. C*, **114**, 3082–3088.
36. Naito, K., Tachikawa, T., Fujitsuka, M., and Majima, T. (2008) Real-time single-molecule imaging of the spatial and temporal distribution of reactive oxygen species with fluorescent probes: applications to TiO_2 photocatalysts, *J. Phys. Chem. C*, **112**(4), 1048–1059.
37. Hirakawa, T., Yawata, K., and Nosaka, Y. (2007) Photocatalytic reactivity for $\bullet O_2^-$ and •OH radical formation in anatase and rutile TiO_2 suspension as the effect of H_2O_2 addition, *Appl. Catal., A*, **325**(1), 105–111.
38. Konovalova, T.A., Lawrence, J., and Kispert, L. D. (2004) Generation of superoxide anion and most likely singlet oxygen in irradiated TiO_2 nanoparticles modified by carotenoids, *J. Photochem. Photobiol., A*, **162**, 1–8.
39. Nosaka, Y., Daimon, T., Nosaka, A.Y., and Murakami, Y. (2004) Singlet oxygen formation in photocatalytic TiO_2 aqueous suspension, *Phys. Chem. Chem. Phys.* **6**, 2917–2918.
40. Daimon, T. and Nosaka, Y. (2007) Formation and behavior of singlet molecular oxygen in TiO_2 photocatalysis studied by detection of near-infrared phosphorescence, *J. Phys. Chem. C*, **111**(11), 4420–4424.
41. Daimon, T., Hirakawa, T., Kitazawa, M., Suetake, J., and Nosaka, Y. (2008) Formation of singlet molecular oxygen associated with the formation of superoxide radicals in aqueous suspensions of TiO_2 photocatalysts, *Appl. Catal., A*, **340**, 169–175.
42. Daimon, T., Hirakawa, T., and Nosaka, Y. (2008) Monitoring the formation and decay of singlet molecular oxygen in TiO_2 photocatalytic systems and the reaction with organic molecules, *Electrochemistry*, **76**(2), 136–139.
43. Konaka, R., Kasahara, E., Dunlap, W. C., Yamamoto, Y., Chien, K. C., and

Inoue, M. (1999) Irradiation of titanium dioxide generates both singlet oxygen and superoxide anion. *Free Radical Biol. Med.*, **27**(3/4), 294–300.

44. Nosaka, Y., Natsui, H., Sasagawa, M., and Nosaka, A. Y. (2006) ESR studies on the oxidation mechanism of sterically hindered cyclic amines in TiO_2 photocatalytic systems, *J. Phys. Chem. B*, **110**(26),12993–12999.

45. Maldotti, A., Molinari, A., and Amadelli, R. (2002) Photocatalysis with organized systems for the oxofunctionalization of hydrocarbons by O_2. *Chem. Rev.* **102** (10), 3811–3836.

46. Clinton, N. A. Kenley, R. A., Traylor, T. G. (1975) Autoxidation of acetaldehyde. III. Oxygen-labeling studies, *J. Am. Chem. Soc.* **97**(13), 3757–3762.

47. Ikeda, K., Sakai, H., Ryo, R., Hashimoto, K., Fujishima, A. (1997) Photocatalytic reactions involving radical chain reactions using microelectrodes, *J. Phys. Chem. B*, **101**(14), 2617–2620.

48. Abe, R., Takami, H., Murakami, N., Ohtani, B. (2008) Pristine simple oxides as visible light driven photocatalysts: highly efficient decomposition of organic compounds over platinum-loaded tungsten oxide, *J. Am. Chem. Soc.*, **130** (25), 7780–7781.

49. Ishibai, Y., Sato, J., Nishikawa, T., Miyagishi, S. (2008) Synthesis of visible-light active TiO_2 photocatalyst with Pt-modification: role of TiO_2 substrate for high photocatalytic activity, *Appl. Catal., B*, **79**, 117–121.

50. Irie, H., Miura, S., Kamiya, K., Hashimoto, K. (2008) Efficient visible light-sensitive photocatalysts: grafting Cu(II) ions onto TiO_2 and WO_3 photocatalysts. *Chem. Phys. Lett.*, **457**, 202–205.

51. Nosaka, Y., Takahashi, S., Sakamoto, H., Nosaka, A. Y. (2011) Reaction mechanism of Cu(II)-grafted visible-light responsive TiO_2 and WO_3 photocatalysts studied by means of ESR spectroscopy and chemiluminescence photometry, *J. Phys. Chem. C* **115**(43), 21283–21290.